

RESEARCH ARTICLE

Self-catalyzed formation of strongly interconnected multiphase molybdenum-based composites for efficient hydrogen evolution

Jiani Chen¹ | Haijuan Zhang¹ | Jie Yu² | Daqin Guan¹ | Sixuan She¹ | Wei Zhou¹  | Zongping Shao^{1,3} 

¹State Key Laboratory of Materials-Oriented Chemical Engineering, College of Chemical Engineering, Nanjing Tech University, Nanjing, China

²Department of Building and Real Estate, Building Energy Research Group, The Hong Kong Polytechnic University, Hong Kong, China

³WA School of Mines: Minerals, Energy and Chemical Engineering (WASM-MECE), Curtin University, Perth, Western Australia, Australia

Correspondence

Wei Zhou and Zongping Shao, State Key Laboratory of Materials-Oriented Chemical Engineering, College of Chemical Engineering, Nanjing Tech University, Nanjing 211816, China.
Email: zhouwei1982@njtech.edu.cn (W. Z.) and shaozp@njtech.edu.cn (Z. S.)

Abstract

Molybdenum carbide (Mo_xC) with variable phase structure possesses flexible hydrogen-binding energy (HBE), which is a promising hydrogen evolution reaction (HER) catalyst. Herein, a hybrid multiphase Mo_xC freestanding film coupled with Co_3Mo ($\text{CM}/\text{Mo}_x\text{C}@\text{NC}$) is synthesized through the electrospinning method supplemented by the heteroatom incorporation. $\text{CM}/\text{Mo}_x\text{C}@\text{NC}$ surpasses its pure phase counterparts and exhibits remarkable catalytic activity at 114 mV to deliver a current density of 10 mA cm^{-2} in acid, which is among the first-rate level performance reported for Mo_xC -based catalysts. The subsequent ex situ and in situ characterizations reveal a phase transition mechanism based on self-catalysis that CoO_x depletes the coordinated C of $\alpha\text{-MoC}$ via the interaction, which realizes the assembly of weak HBE $\alpha\text{-MoC}$ and strong HBE $\beta\text{-Mo}_2\text{C}$, and the enhanced utilization of active materials as well. The multiple structures with optimal HBE are in favor of the stepwise reactions of HER, as the study of the correlation between HBE and phase structure revealed. This study discloses the underlying phase transition mechanism and highlights the HBE–structure relationship that should be considered for catalyst design.

KEYWORDS

hydrogen-binding energy, hydrogen evolution reaction, molybdenum carbide, phase transition, self-catalysis

1 | INTRODUCTION

Hydrogen generation from electrochemical water splitting is an efficient approach to relieve the burgeoning severe energy crisis and environmental problems. As one of the key half-reactions in water splitting, the highly efficient hydrogen evolution reaction (HER) is crucial for the industrial application of electrochemical water splitting.^{1–4}

Platinum-group metals are flagship catalysts for HER, but restricted rare earth reserves and high costs limit their universal application.^{5–7} Molybdenum carbide (Mo_xC) with a Pt-like electronic structure, good conductivity, and corrosion resistance has shown great potential in HER catalysis and is worthy of in-depth exploration.^{8–10}

Since the Leonard group first revealed the HER catalytic performance of Mo_xC in four phases ($\alpha\text{-MoC}$,

This is an open access article under the terms of the Creative Commons Attribution License, which permits use, distribution and reproduction in any medium, provided the original work is properly cited.

© 2021 The Authors. *Carbon Energy* published by Wenzhou University and John Wiley & Sons Australia, Ltd.

β -Mo₂C, η -MoC, and γ -MoC), optimization of the four phases has been relentlessly pursued.¹¹ The four structures of molybdenum carbide are either different in crystal structure or distinguish from the stacking sequence. The synthesis conditions of γ -MoC are relatively harsh, and η -MoC requires up to 1000°C to crystallize, which inevitably brings the drawbacks of excessive accumulation of particles and loss of active sites.^{11,12} Therefore, α -MoC and β -Mo₂C have become the preferred candidates.^{13–15} Morphology regulation provides various well-defined nanostructures, such as nanowires, nanosheets, and nanodendrites, which not only establish directional transmission channels but also introduce more active surfaces.^{16–18} The intrinsic activity of the active sites is yet associated with their adsorption ability with reactants, which refers to the hydrogen-binding energy (HBE) in HER case. Molybdenum carbide with different ratios of Mo to C results in variable electronic properties; in turn, the regulation of the HBE could be achieved.^{19,20} Specifically, β -Mo₂C is the main focus because of its strong HBE (−0.27 eV), which benefits the production of hydrogen bound to active sites. α -MoC is reported to have considerable activity for HER due to its excellent water dissociation capability, but it is limited by its weak HBE, which is estimated to be 0.66 eV in acid.^{21,22} Introducing heteroatoms into parent materials also can effectively trigger the favorable redistribution of electron structure, for instance, electron delocalization and modulating electron feature to Fermi level.^{23,24} It is known that the HER involves the hydrogen adsorption and desorption steps; hence, employing the synergistic functions of different intermediate HER steps between α -MoC and β -Mo₂C is necessary to achieve optimal HBE.²⁵

Furthermore, as a new class of electrocatalysts, freestanding films fabricated by electrospinning require no binders and usually demonstrate excellent electrical conductivity, abundant electrochemical surface area, and fine mechanical stability, which show great promise for applications in advanced electrocatalysts.^{26–29}

Herein, a hybrid HER electrocatalyst of Mo_xC (α -MoC and β -Mo₂C) coupled with intermetallic Co₃Mo loaded on nitrogen-doped carbon nanofiber freestanding films (CM/Mo_xC@NC) was synthesized via an electrospinning method. We report a hetero-incorporation strategy that optimizes the activity of Mo_xC by regulating the hydrogen affinity of active sites as well as the utilization of active material. The in situ and ex situ characterizations further indicated that CoO_x could interact with the coordinated C of α -MoC during crystallization, thereby triggering the phase transition. Benefiting from the self-catalyzed mechanism of the catalyst, different functional adsorption sites were created and contributed to the performance promotion, especially the 47-fold and

4.7-fold increases in mass activity and specific activity, respectively. The freestanding CM/Mo_xC@NC catalyst requires an overpotential of 114 mV at 10 mA cm^{−2} in acid. Furthermore, thanks to the advantages of the freestanding film, the CM/Mo_xC@NC catalyst has potential in industrial applications.

2 | EXPERIMENTAL SECTION

2.1 | Materials

Ammonium molybdate tetrahydrate ((NH₄)₆Mo₇O₂₄·4H₂O), cobalt(II) nitrate hexahydrate (Co(NO₃)₂·6H₂O), citric acid (CA), *N,N*-dimethylformamide (DMF), and 20 wt% Pt/C were purchased from Sinopharm Chemical Reagent Co., Ltd. and other suppliers. Polyacrylonitrile was purchased from Alfa Aesar Co., Ltd. The above chemicals were of analytical grade and used directly.

2.2 | Synthesis of CM/Mo_xC@NC nanofibers precursors

The CM/Mo_xC@NC nanofiber precursors were fabricated by the electrospinning method (SS-2535H, Ucalery). Typically, (NH₄)₆Mo₇O₂₄·4H₂O (3 mmol), Co(NO₃)₂·6H₂O (0.45 mmol), and CA (2 mmol) were dissolved in DMF (10 mL) under vigorous stirring. After the solution became homogeneous, 0.8 g of polyacrylonitrile was added and the resulting solution was stirred for 12 h in 50°C bath oil. The obtained solution was transferred into a 2-mL plastic syringe equipped with a 22-gauge metal nozzle for electrospinning. The applied voltage and distance between the needle tip and the collector were 10 kV and 10 cm, respectively. The solution flow rate was kept at 0.2 mL h^{−1}. The as-spun fibers were collected on a rolling drum wrapped in aluminum foil. The nanofiber precursors of MoC@NC (nitrogen-doped carbon nanofibers with α -MoC embedded) and Mo₂C@NC (nitrogen-doped carbon nanofibers with β -Mo₂C embedded) were prepared through the same process as CM/Mo_xC@NC except that no cobalt source was added.

2.3 | Synthesis of freestanding catalysts

For CM/Mo_xC@NC catalyst, the as-spun fibers were calcined under Ar and H₂/Ar (10% H₂, 90% Ar) atmosphere, respectively. Specifically, the fibers were first calcined under Ar at 800°C for 2 h with a heating rate of 2°C min^{−1} and then cooled to room temperature. After that, the atmosphere was changed to H₂/Ar for the

second calcination step, while keeping the heating rate and temperature consistent. For the MoC@NC sample, the precursors were calcined with the identical heating procedure of CM/Mo_xC@NC but only in the Ar atmosphere. For the Mo₂C@NC sample, the precursors were calcined with the identical procedure of CM/Mo_xC@NC. To achieve the powder sample, the freestanding sample was ground by mortar and pestle subsequently.

2.4 | Electrochemistry

The HER performance of the catalysts was tested on a CHI 760 electrochemical workstation with a standard three-electrode configuration, which was composed of an Ag/AgCl (3.5 M) as reference electrode, a graphite rod as the counter electrode, and the glassy carbon (GC) as a working electrode. All potentials were calibrated to a reversible hydrogen electrode (RHE) according to the equation with *iR* compensation: $E_{\text{RHE}} = E_{\text{Ag/AgCl}} + iR + 0.235 \text{ V}$. The catalyst ink was prepared by dispersing catalyst samples (10 mg) and 10 mg of Super P Li into a mixture of Nafion (100 μL , 5 wt%) and of absolute ethanol (1 mL) followed by sufficient sonication. Then, 5 μL of ink was pipetted onto the GC substrate (0.196 cm^2) and dried naturally, yielding catalyst loading of nearly 0.232 mg cm^{-2} . For the stability test, the freestanding CM/Mo_xC@NC catalyst films were used as working electrodes directly. Before the test, 0.5 M H₂SO₄ electrolyte was bubbled with Ar for at least 30 min.

2.5 | Characterizations

X-ray diffraction (XRD) data was taken from a Rigaku Smartlab 3 kW with Cu-K α radiation ($\lambda = 1.5406 \text{ \AA}$). XRD Rietveld refinement was conducted using the GSAS-EXPGUI for more detailed structural information. Nitrogen adsorption-desorption measurements were conducted on a BELSORP II at 77 K using the Brunauer-Emmett-Teller and Barrett-Joyner-Halenda methods. Thermal gravimetric (TG) curves were collected by an STA 449 F3 Jupiter, NETZSCH. The Raman spectra were attained by a LabRAM HR Evo (HORIBA FRANCE SAS) machine. The microstructure information was investigated by scanning electron microscopy (SEM) (S-4800; Hitachi) and transmission electron microscopy (TEM) (JEM-2100F; JEOL). The concentration of metal elements was quantified by inductively coupled plasma-atomic emission spectroscopy (ICP-AES) (Optima 5300DV; Perkin-Elmer). X-ray photoelectron spectroscopy (XPS) spectra were performed by a PHI5000 VersaProbe spectrometer equipped with an Al K α X-ray source.

3 | RESULTS AND DISCUSSION

The synthesis procedure is illustrated schematically in Figure 1A, and nanofiber freestanding catalysts were successfully synthesized through the electrospinning method followed by specified calcination (see Section 2; Figure S1). The crystal configuration and morphology of MoC@NC and CM/Mo_xC@NC were investigated by XRD and SEM, respectively. Figure 1B shows that a dual-phase Mo_xC composite consisting of β -Mo₂C and α -MoC was obtained for CM/Mo_xC@NC. In addition, the slight peak appearing at 46.4° is attributed to Co₃Mo due to the low doping amounts of Co, whereas a single phase of α -MoC was achieved for MoC@NC. This result indicated that the Co dopant induced the multiphase formation of Mo_xC. The peak at approximately 26° corresponds to the graphitic carbon derived from polyacrylonitrile. Rietveld refinement was carried out to obtain the detailed phase structure of CM/Mo_xC@NC (Figure 1C), in which β -Mo₂C was the dominant phase and accounted for 75.8 wt%, suggesting that the dramatic phase transition was caused by the Co dopant. Figure 1D,E reveals the nanofiber interlinked network nature of the resulting catalysts. Notably, in contrast to the smoothness of MoC@NC, CM/Mo_xC@NC had a relatively rough surface in which nanoparticles were observed. TEM images further presented lattice spacings of 0.27 and 0.25 nm that corresponds to the (100) plane of β -Mo₂C and the (111) plane of α -MoC, respectively (Figure 1F). A spacing of 0.2 nm indexed to the (201) plane of Co₃Mo is also presented in Figure S2, confirming the phase configuration determined through XRD. The inset of Figure 1F clearly displays the nanoparticles precipitated from NCNFs (nitrogen-doped carbon nanofibers) in CM/Mo_xC@NC as marked by circles. Energy-dispersive X-ray mapping (Figure 1G) was conducted to distinguish the distribution of Mo, Co, C, and N in this hybrid. The doping concentration of Co and N were 3.5 and 1.2 wt%, respectively, as summarized in Table S1. The elements Mo and Co were obviously distributed in the exsolved particles, while the overlapping section came from the Co₃Mo compound, and then C was distributed homogeneously, robustly corroborating that the precipitated nanoparticles were Mo_xC and Co₃Mo. Then, the surface configuration schematic of MoC@NC and CM/Mo_xC@NC could be represented, as shown in Figure 1H. With NCNFs as the growth skeleton, MoC@NC maintained a smooth surface as α -MoC nanoparticles were concealed beneath the carbon surface, whereas Mo_xC and Co₃Mo in CM/Mo_xC@NC were partly exposed outside the carbon shell and, thus, easily made contact with the electrolyte. The exposed nanoparticles could create multiple adsorption sites for hydrogen species and prompt the exchange of reactive species.

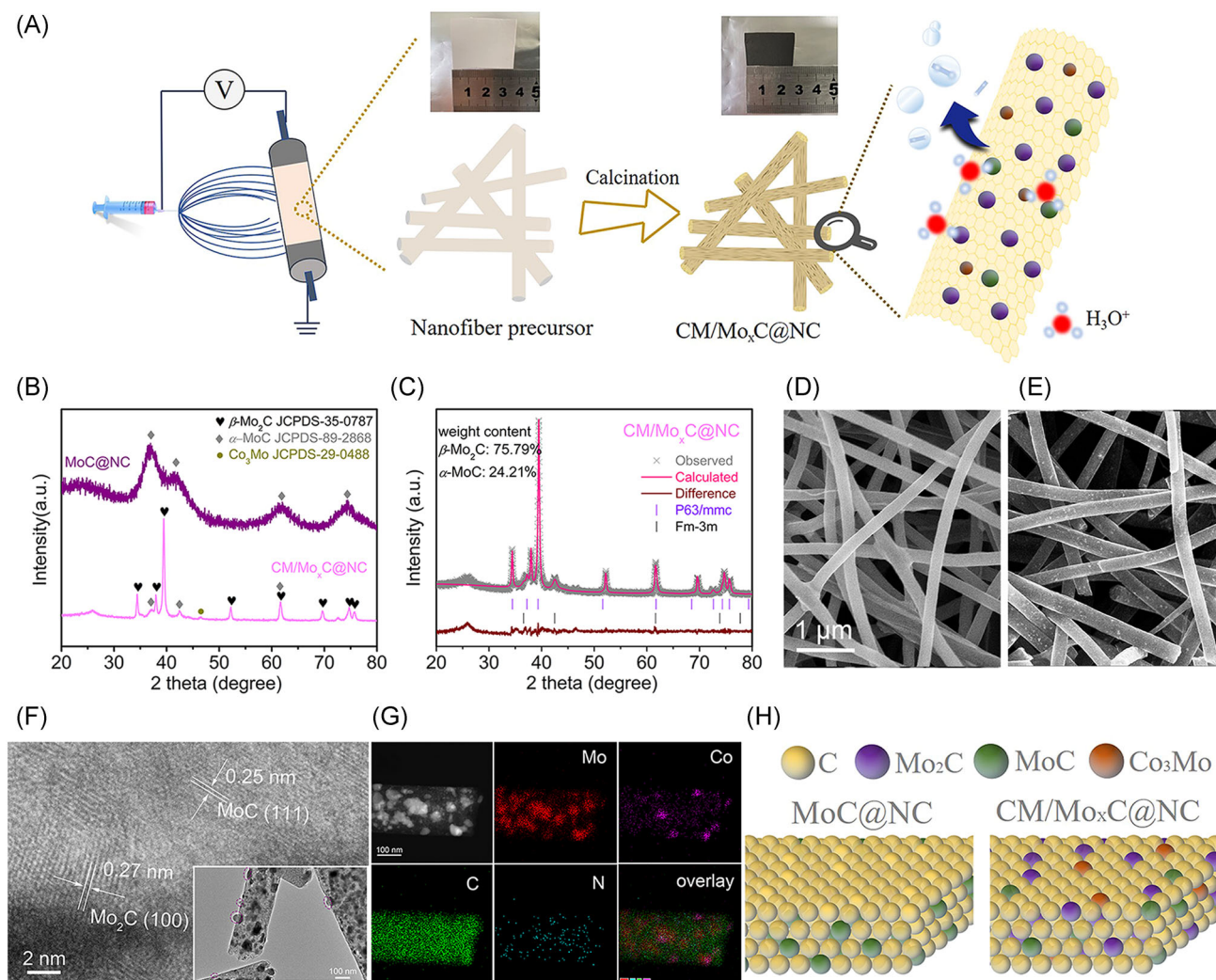


FIGURE 1 (A) Synthesis procedure of CM/Mo_xC@NC. (B) XRD pattern and (C) XRD Rietveld refinement pattern of catalysts. SEM images of (D) MoC@NC and (E) CM/Mo_xC@NC. (F) TEM image and (G) EDX images of CM/Mo_xC@NC. (H) Surface configuration schematic of MoC@NC and CM/Mo_xC@NC. CM/Mo_xC@NC, intermetallic Co₃Mo loaded on nitrogen-doped carbon nanofiber freestanding film; EDX, energy-dispersive X-ray; MoC@NC, nitrogen-doped carbon nanofibers with α -MoC embedded; SEM, scanning electron microscopy; TEM, transmission electron microscopy; XRD, X-ray diffraction

The morphology difference between the two samples impacted their surface area, as revealed by the N₂ adsorption-desorption isotherms (Figure 2A). The catalyst CM/Mo_xC@NC possessed a higher specific surface area and porosity than MoC@NC, displaying its congenital superiority in the active area for HER. The surface electronic states of the samples were also analyzed by XPS. Distinct peaks in the overview survey spectrum (Figure S3) verified the presence of Mo, Co, C, and N. The high-resolution Mo 3d spectrum was deconvoluted into several doublets (Figure 2B) ascribed to Mo²⁺ (228.2/231.2 eV), Mo³⁺ (228.7/231.9 eV), Mo⁴⁺ (230.2/232.9 eV), and Mo⁶⁺ (232.5/235.8 eV). The oxidation states of Mo²⁺ and Mo³⁺ originated from the Mo–C bonds for β -Mo₂C and α -MoC, and Mo⁴⁺ and Mo⁶⁺ were attributed to the surface unavoidable oxidized MoO_x

species.^{11,30} The shift in the spectrum of CM/Mo_xC@NC to lower energy reflected the reduction of Mo valence, in accordance with the formation of low-valent β -Mo₂C. The varying ratios of Mo²⁺ and Mo³⁺ on the catalyst surface also suggested the generation of phase transition, due to the dominance of Mo²⁺ in β -Mo₂C. Such a variation could affect the HER activity, which is electronic state-sensitive. The XPS spectra of Co are presented in Figure 2C in which several types of characteristic peaks, such as metallic Co⁰, Co–N bonds, oxidized Co, and satellite peaks were analyzed, confirming the presence of Co₃Mo and Co–N in the composite.³⁰ N doping was also proven in the N 1s spectrum (Figure S4), which featured the characteristic peaks of pyridinic N, pyrrolic N, graphitic N, and Mo–N coupling center. The thermally induced metal-nitrogen Mo–N and Co–N

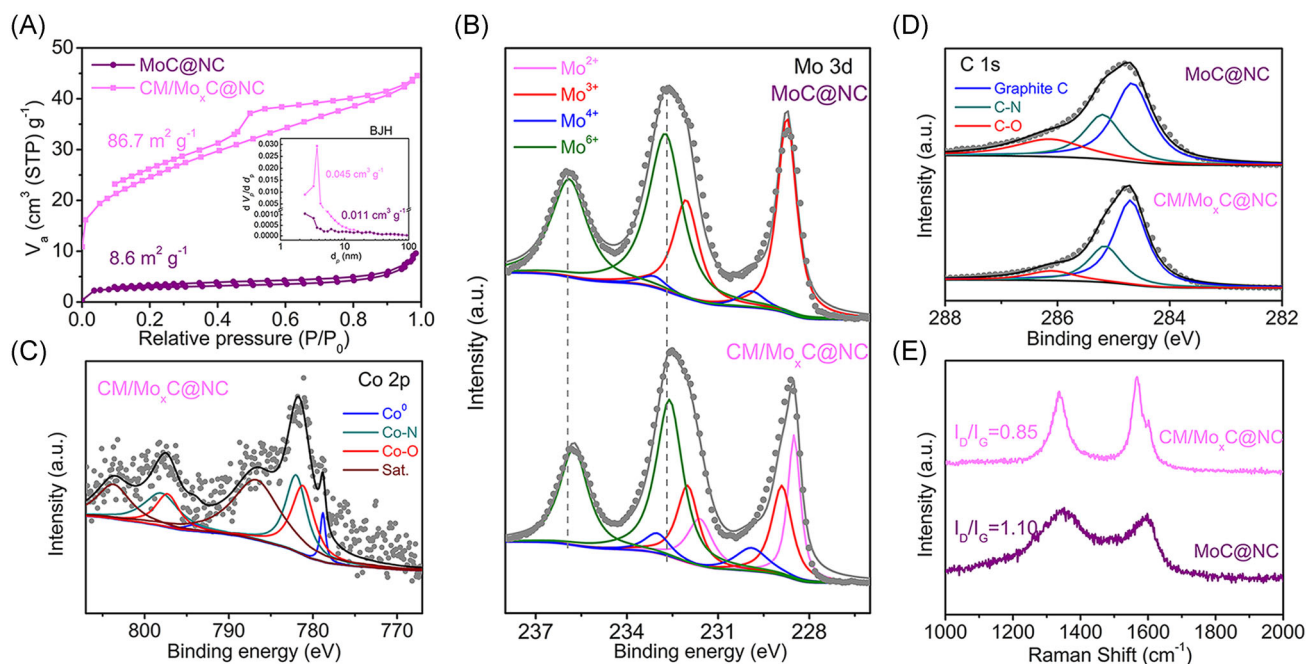


FIGURE 2 (A) N₂ adsorption-desorption isotherms of catalysts. X-ray photoelectron spectra of (B) Mo 3d, (C) Co 2p, and (D) C 1s for different catalysts. (E) Raman spectra of catalysts

bonds are believed to enable a noble-metal-like electronic structure for catalysts and favor catalytic reactions through heterointerfaces with more charge carriers.³¹ Moreover, graphitic N resulting from the incorporation of nitrogen into the carbon skeleton is reported to improve the cooperation between protons and active sites.^{32,33} C-O bonds could cause the disorder of the local *sp*² carbon lattice and hamper the conductivity. However, its content decreased with Co doping, as shown in Figure 2D.³⁴ Raman spectroscopy (Figure 2E) further proved this transformation, and the decreased intensity of I_D/I_G after doping suggested enhanced conductivity and the presence of graphitic carbon, of which the D band and G band were related to defect-induced carbon and graphitic carbon, respectively.

The electrochemical measurements of HER were conducted in an Ar-saturated 0.5 M H₂SO₄ solution equipped with a standard three-electrode system. As CM/Mo_xC@NC has the multiphase structure, the Mo₂C@NC sample was also prepared as the pure β -Mo₂C phase for direct electrocatalytic comparison (Figure S5). The typical polarization curves of the three samples are illustrated in Figure 3A. The CM/Mo_xC@NC showed the best catalytic performance with a low overpotential and large current density. Specifically, the CM/Mo_xC@NC catalyst exhibited a small overpotential (η_{10}) of 149 mV to deliver a 10 mA cm_{disk}⁻² current density, which was 191 mV lower than that of MoC@NC and 59 mV lower than that of Mo₂C@NC. The η_{10} of the freestanding catalyst was 114 mV for CM/Mo_xC@NC (Figure S6), representing an

exceptional performance among the reported Mo_xC-based catalysts (Table S2). The rapid reactant transport endowed by the seamlessly integrated interfacial contact was responsible for the excellent performance of the freestanding catalysts.

Mass activity (MA) is a key factor for practical applications, while specific activity (SA) represents the intrinsic activity of catalysts. Figure 3B shows a visual comparison of MA and SA, which were normalized to the sample mass loading and specific surface area, respectively. The CM/Mo_xC@NC catalyst delivered an enhanced performance for both MA and SA, exhibiting a 47-fold increase in MA and a 4.7-fold increase in SA compared to those of MoC@NC. Moreover, electrochemical double-layer capacitance (*C*_{dl}) calculated from the cyclic voltammetry data (Figure S7) was applied to approximate the electrochemical surface area. As shown in Figure 3C, the *C*_{dl} value of CM/Mo_xC@NC was 5.89 mF cm⁻², exceeding that of MoC@NC (0.67 mF cm⁻²). This result implied that CM/Mo_xC@NC had a larger catalytic area, which was beneficial to the HER performance.³⁵ The smaller Tafel slope of 86 mV dec⁻¹ of CM/Mo_xC@NC compared to that of MoC@NC (136 mV dec⁻¹) demonstrated its favorable reaction kinetics (Figure 3D), related to the HBE as discussed later.

During the durability test, the freestanding nanofiber films were used directly as working electrodes. Chronopotentiometry testing was performed with a constant current density of 10 mA cm⁻². As shown in Figure 3E, the

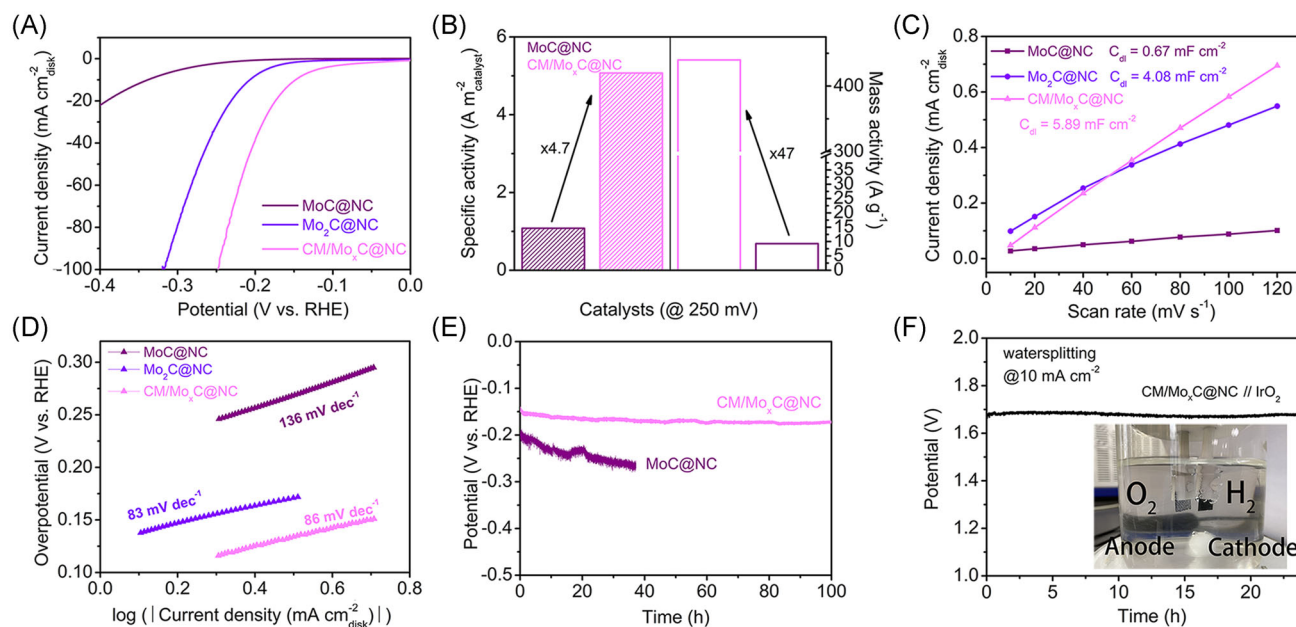


FIGURE 3 (A) HER polarization curves, (B) mass activity and BET surface area normalized specific activity, (C) linear fitting of capacitive currents versus scan rates from cyclic voltammetry tests, and (D) Tafel plots of catalysts in 0.5 M H₂SO₄ solution. The catalyst loading was 0.232 mg cm⁻². (E) Chronopotentiometry curves of CM/Mo₂C@NC nanofilms at a constant cathodic current density of -10 mA cm⁻² for 100 h. (F) Chronopotentiometry curves of water electrolysis using CM/Mo₂C@NC film (-) // IrO₂ (+) couples at 10 mA cm⁻². The mass loading of the IrO₂ electrode was 1.8 mg cm⁻². Inset: a representative photograph of a water-splitting device. BET, Brunauer–Emmett–Teller; CM/Mo₂C@NC, intermetallic Co₃Mo loaded on nitrogen-doped carbon nanofiber freestanding film; EDX, energy-dispersive X-ray; HER, hydrogen evolution reaction

potential of CM/Mo₂C@NC almost held at the original state after 100 h of test, demonstrating its excellent durability. Nitrogen-doped carbon shells are widely believed to be anticorrosive and hereby may provide shelter for Mo₂C and Co₃Mo particles under acidic conditions. Moreover, the freestanding catalysts guarantee fine mechanical properties and avoid catalyst peeling during long-term working, which is a common trouble for electrodes made by drop-casting or spraying catalysts. After the long time working, CM/Mo₂C@NC remained the robust freestanding film in macroscopic view, and it microscopically maintained the interlinked nanofiber network framework without obvious fiber adhesion (Figure S8). A water electrolysis device was also assembled with CM/Mo₂C@NC nanofiber films as the cathode and IrO₂ loaded on carbon cloth as the anode. The polarization curve of the system is shown in Figure S9, and the system displayed 1.63 V to sustain operation at a current density of 10 mA cm⁻². Figure 3F shows that the device was steady for 24 h, reflecting its brilliant capacity for water electrolysis under acidic conditions.

According to the performance test, the generation of multiple phases played a vital role in the performance improvement of molybdenum carbide, and thereby the phase transition mechanism was worth investigating. There are two key variables in this method: the cobalt

salt dopant and temperature. Consequently, we defined the calcination process by tracing the two factors. In the co-calcination with organic precursors, cobalt salts, which are a type of transition metal salt, usually form a Co⁰ nanoparticle-graphitic carbon framework due to interactions between C and CoO_x, the derivative of cobalt salt dopant at high temperature.^{36,37} There is a possibility that the available carbon source, which was supposed to bond with Mo, was depleted by CoO_x, triggering Mo₂C generation. Therefore, determining the reaction target of CoO_x, namely, α -MoC or the carbon source of the framework, is necessary for revealing the phase transition. We chose MoC@NC + CoO, a homogenous mixture of MoC@NC and CoO, as the reference sample and calcined it at a specific temperature. As shown in Figure 4A, the CoO assistant also induced the phase transition from α -MoC to β -Mo₂C if the temperature was sufficient. Specifically, one of the characteristic peaks of the β -Mo₂C (corresponding to (101) plane) first appeared when the temperature increased to 700°C, and the other peaks gradually emerged and enhanced with temperature. Considering that the Mo source was entirely bonded to C in the original MoC@NC + CoO, this evidence suggested that CoO could react with α -MoC and consume the coordinated C in the original lattice, thereby triggering a partial transition from α -MoC to β -Mo₂C. CM/

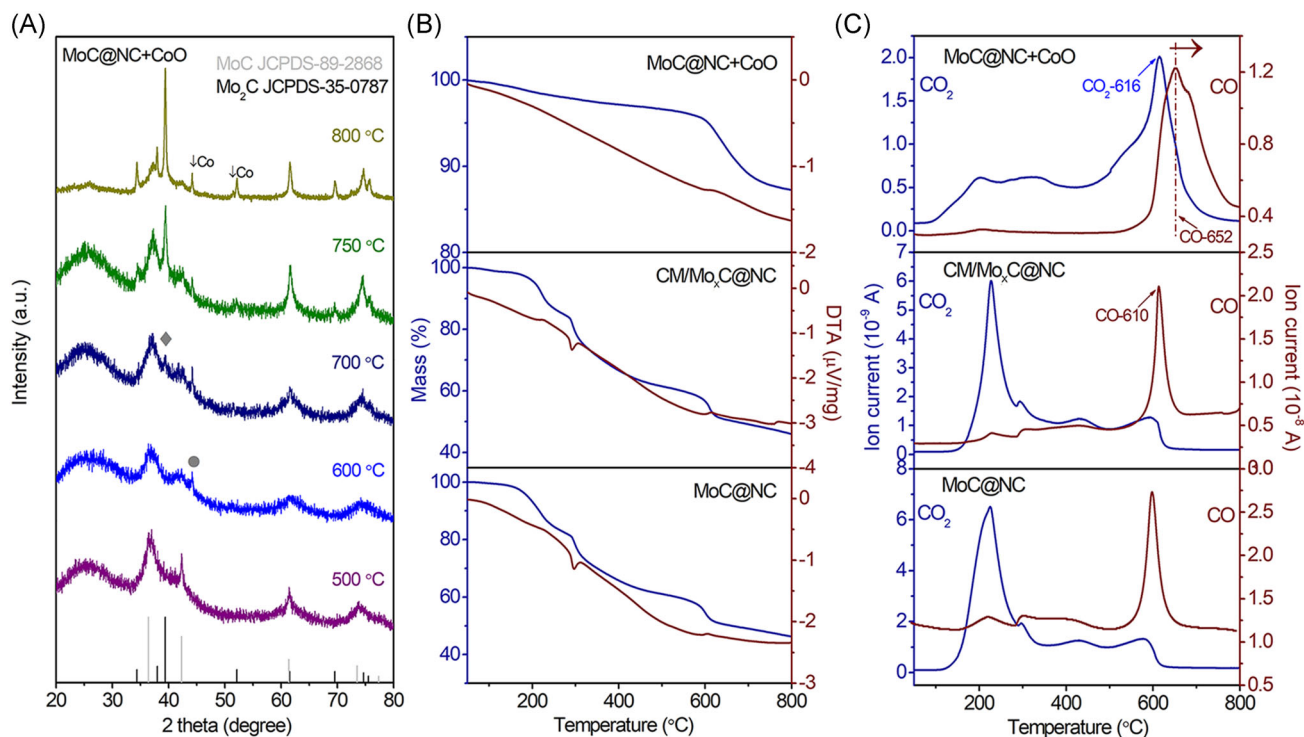
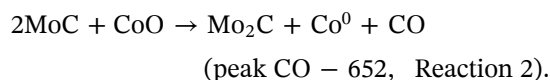
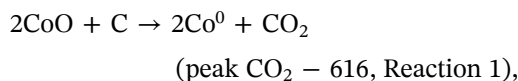


FIGURE 4 (A) X-ray diffraction patterns of the MoC@NC + CoO calcined at specific temperatures. (◆ β -Mo₂C; ● Co). (B) TG-DSC plot and (C) the ion currents for CO₂ and CO of different catalysts. DSC, differential scanning calorimetry; MoC@NC, nitrogen-doped carbon nanofibers with α -MoC embedded; TG, thermogravimetric

Mo_xC@NC had an identical evolution tendency during calcination, as shown in Figure S10, in which the α -MoC phased at 600°C transformed into a composite of α -MoC and β -Mo₂C at 700°C. Note that the metal Co was finally generated in the MoC@NC + CoO case instead of the alloy Co₃Mo in CM/Mo_xC@NC. This observation could be ascribed to the intimate and extensive contact between the Co and Mo sources in the nanofiber precursors, which benefited the bonding of metals during calcination. Hence, the method followed the cobalt-catalyzed mechanism, that is, CoO_x assistant could act as an inducer to initiate the transition of α -MoC to β -Mo₂C by consuming the coordinated C, whether as external additives or raw sources.

TG-mass spectrometry was applied for the in situ detection of gaseous products in calcination to better understand the evolution of carbon, which was an indispensable participant in the phase transition. Featuring electrospun nanofibers, every stage of calcination of MoC@NC and CM/Mo_xC@NC was similar, ending with approximately 50% residue, as shown in Figure 4B. Both the CO₂ signal intensity and differential thermal analysis curves presented a bulge at 230°C (Figure 4C), which was ascribed to the precarbonization of polyacrylonitrile accompanied by 15% weight loss. As the oxygen component in the precursor was gradually consumed, the concentration of CO₂ decreased,

and CO became the primary product. Particularly, it is known that 600°C is generally the temperature where carbonization begins, and an abrupt CO peak at approximately 610°C appeared in the spectra of both MoC@NC and CM/Mo_xC@NC (denoted as CO-610); this evidence was corroborated by the low crystalline carbon XRD peak at 26° in Figure S10.³⁸ In the oxygen-abundant MoC@NC + CoO, the intensity of the CO₂ peak continued to rise and reached a maximum around 616°C (CO₂-616), followed by the conspicuous peak of CO at 652°C (CO-652). Combining the newly emerging XRD signal in the temperature range from 600°C to 700°C (Figure 4A), it can be inferred that Co⁰ was generated by Reaction 1 related with CO₂-616, while β -Mo₂C was born from the reaction between CoO and α -MoC (Reaction 2), together with the byproduct CO, as reflected by peak CO-652.



On the basis of the cobalt-catalyzed mechanism, in CM/Mo_xC@NC case, Reaction 2 was also responsible for

the phase transition. The peak CO-610 in CM/Mo_xC@NC spectrum was a result of both carbonization and Reaction 2, indicating the combination of crystallization and phase transformation. Compared with that of MoC@NC + CoO, the lower starting temperature of Reaction 2 for CM/Mo_xC@NC implied the advantage of self-catalysis that the inherent CoO_x further lowered the threshold of phase transformation. However, the ex situ CoO_x source preferred to react with the carbon framework. The sample MoC@NC + CoO calcined at 800°C was also tested for HER activity (Figure S11), though it exhibited inferior performance to that of CM/Mo_xC@NC. It should be attributed to the in situ-derived multiphase interface of CM/Mo_xC@NC that provided potential active sites and charge carriers, corroborating the superiority of self-catalysis.

Therefore, the formation mechanism of CM/Mo_xC@NC based on the self-catalyzed phase transition could be divided into three steps (Figure 5A). In the first step, the material sources were uniformly mixed in the precursor nanofibers, followed by the prior appearance of α-MoC when the temperature reached 600°C. Finally, the pre-existing CoO_x interacted with the coordinated C in the α-MoC lattice to induce the formation of β-Mo₂C, along with the byproduct CO. In addition, the remaining few Co

sources bonded with Mo to form Co₃Mo; this is considered with high intrinsic activity, as the Mo site reveals oxyphilic and absorbed hydrogen species efficiently.^{39,40} As Figure S12 shows, the mentioned nanoparticle precipitation occurred during the second stage, indicating that the exposure of active sites was closely related to the reaction of cobalt salt dopant, which promoted the utilization of active materials. As the adsorption of reactants on the surface is a prerequisite for catalysis, the precipitation introduced more exposed active sites, which changed the barren adsorption of the original NCNFs with weak HBE and benefited the Volmer step (the adsorption step).⁴¹ According to the empirical value, the limiting Tafel slope of 116 mV dec⁻¹ is an indicator of adsorption-limited reaction, which corresponded to MoC@NC.^{42,43} Nevertheless, CM/Mo_xC@NC possessed a smaller Tafel slope, suggestive of its enhanced HBE and Volmer–Heyrovsky reaction pathway during HER (Figure 5B).

To obtain profound insight into the role of HBE in HER activity, we conducted the underpotential-deposited *H* (*H*_{upd}) method to evaluate the surface electrochemical behavior of three samples.⁴⁴ The position of *H*_{upd} peak (between 0 and 0.3 V, as reported) is directly correlated with the HBE of active sites. Such a correlation provides

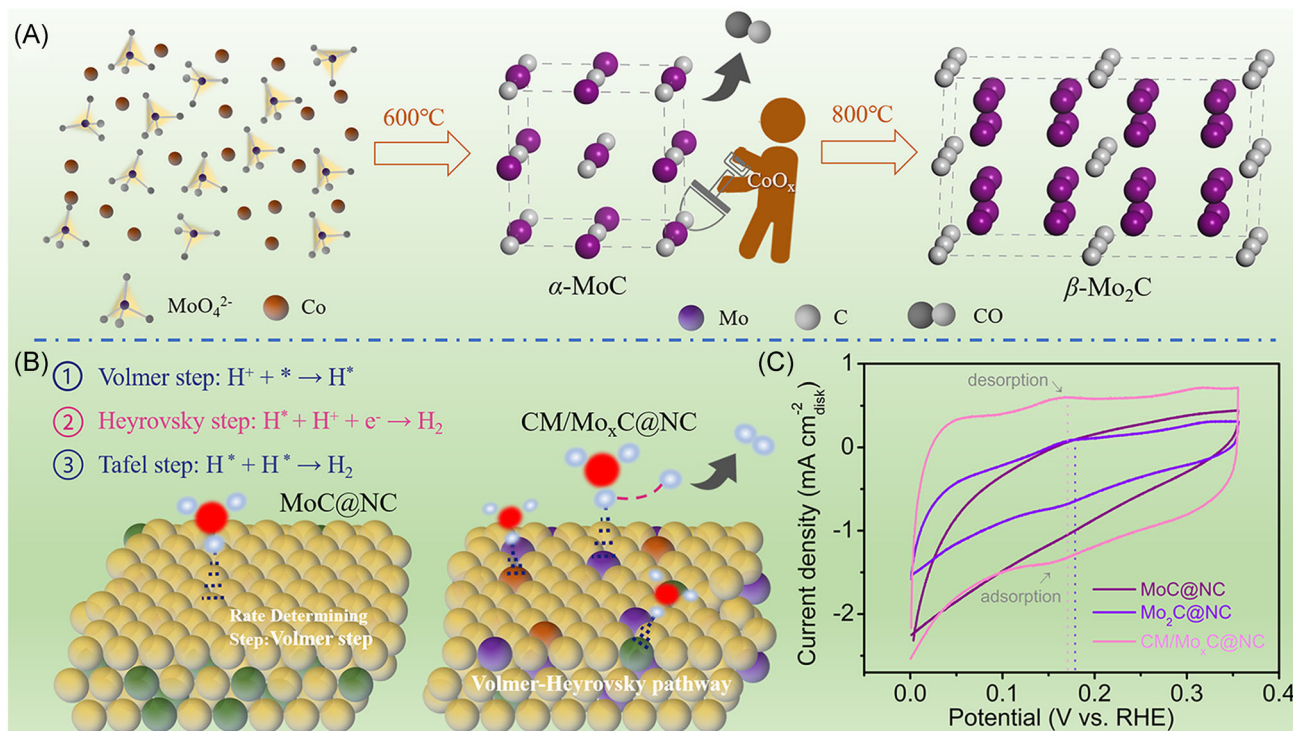


FIGURE 5 Schematic illustration of (A) the growth process of CM/Mo_xC@NC and (B) the reaction pathways on two-type catalysts for acidic HER electrocatalysis. Balls in purple, green, yellow, and orange represent Mo₂C, MoC, C, and Co₃Mo, respectively. (C) Cyclic voltammograms of catalysts measured in Ar-saturated 0.5 M H₂SO₄ at a scan rate of 50 mV s⁻¹. CM/Mo_xC@NC, intermetallic Co₃Mo loaded on nitrogen-doped carbon nanofiber freestanding film; EDX, energy-dispersive X-ray; HER, hydrogen evolution reaction; RHE, reversible hydrogen electrode

a convenient and potent choice to reveal the underlying connection between HBE and structure. The H_{upd} desorption peak was selected for analysis due to its anti-interference.⁴⁵ As Figure 5C shows, the adsorption-desorption peak of MoC@NC was too feeble to be identified, matching its minor hydrogen affinity. The H_{upd} desorption peak of CM/Mo_xC@NC showed a cathodic shift to 0.167 V compared to that of Mo₂C@NC, which was closer to the desorption peak of benchmarking catalyst Pt/C (0.15 V, Figure S13). It can be attributed to the valid combination with weak HBE α -MoC. The result explained the experimentally observed enhanced HER performance, suggesting that the multiple structures can effectively regulate the HBE for superior performance.

4 | CONCLUSION

In summary, it is demonstrated that the regulation of phase structure is an efficient way for molybdenum carbide to significantly improve HER performance. As a proof-of-concept example, the mass activity of CM/Mo_xC@NC was maximally 47-fold that of its pure phase counterpart. The phase transition based on a self-catalyzed mechanism resulted in more exposure of active sites and the multiple structures, which were composed of the weak HBE α -MoC and strong HBE β -Mo₂C. As the study of correlation between HBE and phase structure revealed, the moderate HBE endowed by multiphase abolished the hydrogen adsorption step limitation and contributed to the enhanced activity. This study provides ideas for the development of advanced catalysts from the perspective of the relationship of HBE and structure.

ACKNOWLEDGMENT

This study was supported by the Priority Academic Program Development of Jiangsu Higher Education Institutions (PAPD).

CONFLICT OF INTEREST

The authors declare no conflict of interest.

ORCID

Wei Zhou  <https://orcid.org/0000-0003-0322-095X>

Zongping Shao  <https://orcid.org/0000-0002-4538-4218>

REFERENCES

- Kou T, Wang S, Li Y. Perspective on high-rate alkaline water splitting. *ACS Mater Lett*. 2021;3(2):224-234.
- Sun H, Dai J, Zhou W, Shao Z. Emerging strategies for developing high-performance perovskite-based materials for electrochemical water splitting. *Energy Fuels*. 2020;34(9):10547-10567.
- Yu J, Ran R, Zhong Y, Zhou W, Ni M, Shao Z. Advances in porous perovskites: synthesis and electrocatalytic performance in fuel cells and metal-air batteries. *Energy Environ Mater*. 2020;3(2):121-145.
- Huang ZF, Song J, Du Y, et al. Optimizing interfacial electronic coupling with metal oxide to activate inert polyaniline for superior electrocatalytic hydrogen generation. *Carbon Energy*. 2019;1(1):77-84.
- Deng X, Zhang J, Fan Z, et al. Understanding and engineering of multiphase transport processes in membrane electrode assembly of proton-exchange membrane fuel cells with a focus on the cathode catalyst layer: a review. *Energy Fuels*. 2020;34(8):9175-9188.
- Zhou L, Deng X, Lu Q, Yang G, Zhou W, Shao Z. Zeolitic imidazolate framework-derived ordered Pt-Fe intermetallic electrocatalysts for high-performance Zn-air batteries. *Energy Fuels*. 2020;34(9):11527-11535.
- Jeon TY, Yu SH, Yoo SJ, Park HY, Kim SK. Electrochemical determination of the degree of atomic surface roughness in Pt-Ni alloy nanocatalysts for oxygen reduction reaction. *Carbon Energy*. 2021;3(2):375-383.
- Geng D, Zhao X, Chen Z, et al. Direct synthesis of large-area 2D Mo₂C on in situ grown graphene. *Adv Mater*. 2017;29(35):1700072.
- Wu HB, Xia BY, Yu L, Yu XY, Lou XW. Porous molybdenum carbide nano-octahedrons synthesized via confined carburization in metal-organic frameworks for efficient hydrogen production. *Nat Commun*. 2015;6:6512.
- Sun H, Xu X, Song Y, Zhou W, Shao Z. Designing high-valence metal sites for electrochemical water splitting. *Adv Funct Mater*. 2021;31(16):2009779.
- Wan C, Regmi YN, Leonard BM. Multiple phases of molybdenum carbide as electrocatalysts for the hydrogen evolution reaction. *Angew Chem Int Ed*. 2014;53(25):6407-6410.
- Wang S, Wang J, Zhu M, et al. Molybdenum-carbide-modified nitrogen-doped carbon vesicle encapsulating nickel nanoparticles: a highly efficient, low-cost catalyst for hydrogen evolution reaction. *J Am Chem Soc*. 2015;137(50):15753-15759.
- Li M, Zhu Y, Wang H, Wang C, Pinna N, Lu X. Ni strongly coupled with Mo₂C encapsulated in nitrogen-doped carbon nanofibers as robust bifunctional catalyst for overall water splitting. *Adv Energy Mater*. 2019;9(10):1803185.
- Baek DS, Jung GY, Seo B, et al. Ordered mesoporous metastable α -MoC_{1-x} with enhanced water dissociation capability for boosting alkaline hydrogen evolution activity. *Adv Funct Mater*. 2019;29(28):1901217.
- Zhang H, Jin H, Yang Y, et al. Understanding the synergetic interaction within α -MoC/ β -Mo₂C heterostructured electrocatalyst. *J Energy Chem*. 2019;35:66-70.
- Zhang H, Guan D, Gao X, et al. Morphology, crystal structure and electronic state one-step co-tuning strategy towards developing superior perovskite electrocatalysts for water oxidation. *J Mater Chem A*. 2019;7(33):19228-19233.
- Lu Q, Guo Y, Mao P, et al. Rich atomic interfaces between sub-1 nm RuO_x clusters and porous Co₃O₄ nanosheets boost oxygen electrolysis bifunctionality for advanced Zn-air batteries. *Energy Stor Mater*. 2020;32:20-29.
- Wakerley D, Lamaison S, Ozanam F, et al. Bio-inspired hydrophobicity promotes CO₂ reduction on a Cu surface. *Nat Mater*. 2019;18(11):1222-1227.

19. Yu GQ, Huang BY, Chen X, Wang D, Zheng F, Li XB. Uncovering the surface and phase effect of molybdenum carbides on hydrogen evolution: a first-principles study. *J Phys Chem C*. 2019;123(36):21878-21887.
20. Guan D, Zhou J, Huang YC, et al. Screening highly active perovskites for hydrogen-evolving reaction via unifying ionic electronegativity descriptor. *Nat Commun*. 2019;10:3755.
21. Zhang X, Wang J, Guo T, et al. Structure and phase regulation in Mo_xC ($\alpha\text{-MoC}_{1-x}/\beta\text{-Mo}_2\text{C}$) to enhance hydrogen evolution. *Appl Catal B*. 2019;247:78-85.
22. Michalsky R, Zhang YJ, Peterson AA. Trends in the hydrogen evolution activity of metal carbide catalysts. *ACS Catal*. 2014;4(5):1274-1278.
23. Zhu Y, Tahini HA, Zhou J, et al. Tailored brownmillerite oxide catalyst with multiple electronic functionalities enables ultrafast water oxidation. *Chem Mater*. 2021;33(13):5233-5241.
24. Lin H, Liu N, Shi Z, Guo Y, Tang Y, Gao Q. Cobalt-doping in molybdenum-carbide nanowires toward efficient electrocatalytic hydrogen evolution. *Adv Funct Mater*. 2016;26(31):5590-5598.
25. Dinh CT, Jain A, de Arquer FPG, et al. Multi-site electrocatalysts for hydrogen evolution in neutral media by destabilization of water molecules. *Nat Energy*. 2019;4(2):107-114.
26. Meng X, Deng X, Zhou L, et al. A highly ordered hydrophilic-hydrophobic Janus bi-functional layer with ultralow Pt loading and fast gas/water transport for fuel cells. *Energy Environ Mater*. 2021;4(1):126-133.
27. Ji D, Peng S, Safanama D, et al. Design of 3-dimensional hierarchical architectures of carbon and highly active transition metals (Fe, Co, Ni) as bifunctional oxygen catalysts for hybrid lithium-air batteries. *Chem Mater*. 2017;29(4):1665-1675.
28. Yu L, Zhu Q, Song S, et al. Non-noble metal-nitride based electrocatalysts for high-performance alkaline seawater electrolysis. *Nat Commun*. 2019;10:5106.
29. Song W, Li M, Wang C, Lu X. Electronic modulation and interface engineering of electrospun nanomaterials-based electrocatalysts toward water splitting. *Carbon Energy*. 2021;3(1):101-128.
30. Ouyang T, Ye YQ, Wu CY, Xiao K, Liu ZQ. Heterostructures composed of N-doped carbon nanotubes encapsulating cobalt and $\beta\text{-Mo}_2\text{C}$ nanoparticles as bifunctional electrodes for water splitting. *Angew Chem Int Ed*. 2019;58(15):4923-4938.
31. Zhu Y, Chen G, Xu X, Yang G, Liu M, Shao Z. Enhancing electrocatalytic activity for hydrogen evolution by strongly coupled molybdenum nitride@nitrogen-doped carbon porous nano-octahedrons. *ACS Catal*. 2017;7(5):3540-3547.
32. Jin H, Gu Q, Chen B, et al. Molten salt-directed catalytic synthesis of 2D layered transition-metal nitrides for efficient hydrogen evolution. *Chem*. 2020;6(9):2382-2394.
33. Ortiz-Medina J, Wang Z, Cruz-Silva R, et al. Defect engineering and surface functionalization of nanocarbons for metal-free catalysis. *Adv Mater*. 2019;31(13):1805717.
34. Li D, Jia Y, Chang G, et al. A defect-driven metal-free electrocatalyst for oxygen reduction in acidic electrolyte. *Chem*. 2018;4(10):2345-2356.
35. Hu B, Deng X, Zhou L, et al. Facile synthesis of synergistic Pt/(Co-N)@C composites as alternative oxygen-reduction electrode of PEMFCs with attractive activity and durability. *Compos B Eng*. 2020;193:108012.
36. Ha Y, Fei B, Yan X, et al. Atomically dispersed Co-pyridinic N-C for superior oxygen reduction reaction. *Adv Energy Mater*. 2020;10(46):2002592.
37. Wu C, Liu D, Li H, Li J. Molybdenum carbide-decorated metallic cobalt@nitrogen-doped carbon polyhedrons for enhanced electrocatalytic hydrogen evolution. *Small*. 2018;14(16):1704227.
38. Han S, Feng Y, Zhang F, et al. Metal-phosphide-containing porous carbons derived from an ionic-polymer framework and applied as highly efficient electrochemical catalysts for water splitting. *Adv Funct Mater*. 2015;25(25):3899-3906.
39. Shi H, Zhou YT, Yao RQ, et al. Spontaneously separated intermetallic Co_3Mo from nanoporous copper as versatile electrocatalysts for highly efficient water splitting. *Nat Commun*. 2020;11:2940.
40. Chen J, Ge Y, Feng Q, et al. Nesting Co_3Mo binary alloy nanoparticles onto molybdenum oxide nanosheet arrays for superior hydrogen evolution reaction. *ACS Appl Mater Interfaces*. 2019;11(9):9002-9010.
41. Gerber IC, Serp P. A theory/experience description of support effects in carbon-supported catalysts. *Chem Rev*. 2020;120(2):1250-1349.
42. Xu X, Chen Y, Zhou W, et al. A perovskite electrocatalyst for efficient hydrogen evolution reaction. *Adv Mater*. 2016;28(30):6442-6448.
43. Seh ZW, Kibsgaard J, Dickens CF, Chorkendorff I, Nørskov JK, Jaramillo TF. Combining theory and experiment in electrocatalysis: insights into materials design. *Science*. 2017;355(6321):eaad4998.
44. Zhang J, Wang T, Liu P, et al. Efficient hydrogen production on MoNi_4 electrocatalysts with fast water dissociation kinetics. *Nat Commun*. 2017;8:15437.
45. Zheng J, Zhuang Z, Xu B, Yan Y. Correlating hydrogen oxidation/evolution reaction activity with the minority weak hydrogen-binding sites on Ir/C catalysts. *ACS Catal*. 2015;5(7):4449-4455.

AUTHOR BIOGRAPHIES



Jiani Chen was born in Jiangsu, China in 1996. She obtained her bachelor's degree in Nanjing Tech University in 2014. She is pursuing her Ph.D. degree in Nanjing Tech University, majoring in chemical engineering. Now her research interest mainly focuses on exploring advanced materials for energy storage and conversion.



Wei Zhou was born in 1982 in Nanjing, China. He earned his Ph.D. degree from Nanjing Tech University in 2009, where he carried out research on the development and synthesis of high-performance cathode materials for solid-oxide fuel cells. He was awarded Australian Postdoctoral Fellow to work at the University of Queensland in 2010, and

then he was promoted to research fellow in 2013. In 2015, he became a professor at Nanjing Tech University. His research interests include the development of key materials for low-temperature SOFCs; electrocatalysts for the ORR/OER/HER; MIECs for wastewater treatment; and scale-up of direct carbon fuel-cell stacks.



Zongping Shao is a professor of chemical engineering at Nanjing Tech University, China, and Curtin University, Australia. He obtained his Ph.D. degree from Dalian Institute of Chemical Physics, China, in 2000. He worked as a visiting scholar at the Institute de Recherches sur la Catalyse et l'Environnement de Lyon (IRCELY N), CNRS, France, and postdoctorate at the California Institute of Technology, USA, from 2000 to 2005.

His current research interests include solid-oxide fuel cells, lithium-ion batteries, oxygen-permeable membranes, and low-temperature energy conversion devices.

SUPPORTING INFORMATION

Additional Supporting Information may be found online in the supporting information tab for this article.

How to cite this article: Chen J, Zhang H, Yu J, et al. Self-catalyzed formation of strongly interconnected multiphase molybdenum-based composites for efficient hydrogen evolution.

Carbon Energy. 2022;4:77-87.

<https://doi.org/10.1002/cey2.156>